α particle preformation and shell effect for heavy and superheavy nuclei*

Yan-Wei Zhao(赵言炜)[1] Shu-Qing Guo(郭树青)[1] Hong-Fei Zhang(张鸿飞)[1,2;1)]

[1] School of Nuclear Science and Technology, Lanzhou University, Lanzhou 730000, China
[2] Joint Department for Nuclear Physics, Lanzhou University and Institute of Modern Physics, CAS, Lanzhou 730000, China

Abstract: The α particle preformation factor is extracted within a generalized liquid drop model for $Z = 84$ - 92 isotopes and $N = 126$, 128, 152, 162, 176, 184 isotones. The calculated results show clearly that the shell effects play a key role in α particle preformation. The closer the proton and neutron numbers are to the magic numbers, the more difficult the formation of the α cluster inside the mother nucleus is. The preformation factors of the isotopes reflect that $N = 126$ is a magic number for Po, Rn, Ra, and Th isotopes, but for U isotopes the weakening of the influence of the N =126 shell closure is evident. The trend of the factors for $N = 126$ and $N = 128$ isotones also support this conclusion. We extend the calculations for $N = 152$, 162, 176, 184 isotones to explore the magic numbers for heavy and superheavy nuclei, which are probably present near $Z = 108$ to $N = 152$, 162 isotones and $Z = 116$ to $N = 176$, 184 isotones. The results also show that another subshell closure may exist after $Z = 124$ in the superheavy nuclei. This is useful for future experiments.

Keywords: α particle preformation, generalized liquid drop model, shell effect, magic number

PACS: 21.10.Tg, 23.60.+e, 27.90.+b **DOI:** 10.1088/1674-1137/42/7/074103

1 Introduction

α emission is one of the most significant decay channels of heavy nuclei. Its experimental measurements can offer reliable information on nuclear structures, for instance, the nuclear spin and parity, nuclear clustering, the nuclear interaction, the shell effects, the nuclear deformation, the ground-state half-life, and the ground-state energy [1–9]. Since reliable information on the mother nucleus can be extracted from α decay, these kinds of measurements can also be used to identify new heavy elements and nuclides [10–13]. With the development of low temperature detectors and radioactive beam technology, there is renewed interest in α decay.

Gamow, Condon and Gurney first explained the α decay process as a quantum tunneling effect in the 1920s [14, 15], which is one of the earliest instances proving the necessity of describing nuclear phenomena and properties with quantum mechanics. The absolute α decay width was predicted after the theoretical calculations were built. The results of the calculations can also be used to extract relevant information about nuclei and to further explore the α-decay phenomenon on the meta-microscale. Various theoretical models such as the cluster model, the fission-like model and the shell model [16–30] were developed to study α decay. The decay constant λ is the product of the the barrier penetrability P, the assault frequency ν_0 and the preformation probability P_0 in the α cluster model. The WKB approximation can describe the barrier penetrability P successfully. Thus, the problem that remains to be solved is how to calculate the preformation probability P_0 of the α decay. It depends strongly on the structures of the mother and daughter nuclei, and it can also show the degree of similarity between the initial state of the mother nucleus and the final state of the daughter nucleus and the α particle [31]. The preformation factor, which is of great importance from the viewpoint of the nuclear structure, is extracted from the experimental α decay half-life T_α when there are experimental data available, or from the reliable theoretical models otherwise.

Magic numbers are involved in the process of evolution of diverse nuclei. Recently, the new neutron-deficient isotope ^{216}U was produced in the complete-fusion reaction ^{180}W(^{40}Ar ,$4n$)^{216}U [32] and the $N = 130$ isotope ^{223}Np was produced in the fusion reaction ^{40}Ar $+^{187}$Re [33], which indicated the absence of the $Z = 92$ subshell closure near $N = 126$. The spurious shell clo-

Received 1 February 2018, Revised 9 April 2018, Published online 18 May 2018

∗ Supported by National Natural Science Foundation of China (11675066, 11475050), Fundamental Research Funds for the Central Universities (lzujbky-2017- ot04) and Feitian Scholar Project of Gansu Province

1) E-mail: zhanghongfei@lzu.edu.cn

sures of $Z=92$ and others can be cured in the upgraded covariant density functional (CDF) model by including ρ-tensor Fock terms, restoring the pseudo-spin symmetry which qualitatively represents the balance of nuclear forces. However, the very recent experimentally observed sudden decrease of the reduced α-decay width at $Z=92$ along the $N=130$ isotonic chain cannot exclude the possibility of a subshell closure at $Z=92$ for $N>126$. The spins and parities of the $N=128$ and 130 isotones were all determined to be $9/2^-$ for odd-Z between 83 and 91, including ^{219}Pa, the daughter nucleus of ^{223}Np, indicating that the odd proton is filling the $\pi h_{9/2}$ orbital up to Pa. They decay to the ground states of their daughters and no fine structures were observed. Around $Z=92$, the proton Fermi surface is closest to the $h_{9/2}$ and $f_{7/2}$ orbitals. The spin of ^{223}Np is expected to be different if a subshell closure exists at $Z=92$, while not vice versa. The trend in proton separation energy shows no sign of a $Z=92$ subshell closure. The spin and parity of ^{223}Np are proposed to be $9/2^-$ by combining the reduced α-decay width and large-scale shell-model calculations in truncated model space, negating the presence of a $h_{9/2}$ subshell closure at $Z=92$ near $N=126$ [32, 33].

The results of the above experiments give us strong motivation to study the shell closure effects of different isotopes and isotones, especially $N=126$ for $Z=92$. The purpose of the present work is to explore what we are interested in as previously mentioned, and to predict the magic numbers of superheavy nuclei by the extracted preformation factors, which has great significance for guiding experiments.

The paper is organized as follows. In Section 2, the calculation methods of the preformation factor, the assault frequencies and the penetrability are shown. In Section 3 the results are presented and discussed, and in Section 4, the conclusions are given and future work is proposed.

2 Theoretical methods

The α decay constant is calculated by

$$\lambda=P_0\nu_0P. \tag{1}$$

The velocity of the α particle is $\nu=\sqrt{\frac{2E_\alpha}{M}}$,

$$\nu_0=\frac{1}{2R}\sqrt{\frac{2E_\alpha}{M}}, \tag{2}$$

R is the radius of the parent nucleus, calculated by

$$R_i=(1.28A_i^{1/3}-0.76+0.8A_i^{-1/3})\ \text{fm}, \tag{3}$$

E_α is the alpha particle energy, which is corrected for recoil, and M is its mass. Using the WKB approximation, one can calculate the penetration probability P. The generalized liquid drop model (GLDM), including the surface, volume, Coulomb and proximity energies, controls the potential barrier to the α emission [34]:

$$E=E_v+E_s+E_c+E_{\text{prox}}. \tag{4}$$

While the nuclei are separated:

$$E_s=17.9439[(1-2.6I_1^2)A_1^{2/3}+(1-2.6I_2^2)A_2^{2/3}]\ \text{MeV}, \tag{5}$$

$$E_v=-15.494[(1-1.8I_1^2)A_1+(1-1.8I_2^2)A_2]\ \text{MeV}, \tag{6}$$

$$E_c=0.6e^2Z_1^2/R_1+0.6e^2Z_2^2/R_2+e^2Z_1Z_2/r, \tag{7}$$

where Z_i, A_i, I_i and R_i are respectively the charge numbers, the mass numbers, the relative neutron excesses and the radii of the two nuclei. r is the distance from one mass center to the other. The radii R_i are calculated by Eq. (3). For one-body shapes, the Coulomb and the surface energies can be calculated by [20, 21, 34]:

$$E_c=0.6e^2(Z^2/R_0)\times0.5\int(V(\theta)/V_0)(R(\theta)/R_0)^3\sin\theta\mathrm{d}\theta, \tag{8}$$

$$E_s=17.9439(1-2.6I_1^2)A^{2/3}(S/4\pi R_0^2)\ \text{MeV}, \tag{9}$$

where V_0 is the surface potential of the sphere, $V(\theta)$ is the electrostatic potential at the surface and S is the surface of the one-body deformed nucleus which results from the surface tension force effects. The proximity energy must be added as an additional term in the nuclear forces between the close surfaces when the nucleons are regarded as a gap or a neck between separated fragments. This parameter is of great significance to describe the smooth transition from one-body to two-body, while reliable fusion barrier heights can also be extracted. It changes the barrier top to an external position and strongly decreases the pure Coulomb barrier:

$$E_{\text{Prox}}(r)=2\gamma\int_{h_{\min}}^{h_{\max}}\Phi[D(r,h)/b]2\pi h\mathrm{d}h, \tag{10}$$

where h is the distance which is different from zero to the height of the neck border or the neck radius. D is the distance of the surfaces and b is the surface width, equal to 0.99 fm. Φ is the proximity function. The surface parameter γ is the geometrical mean between the surface parameters of the two fragments. To combine the generalized liquid drop model (GLDM) with a quasimolecular shape sequence, we can reproduce various data of α decay, for instance, the radii, the heights of fusion barrier, the α, the cluster and the fission radioactivity. The barrier penetrability P can be calculated within the action integral:

$$P=\exp\left[-\frac{2}{\hbar}\int_{R_{\text{in}}}^{R_{\text{out}}}\sqrt{2B(r)(E(r)-E(\text{sphere}))}\right], \tag{11}$$

where E(sphere) is the energy of the spherical nuclei. The two following approximations can be used: $R_{\text{in}}=$

R_d+R_α and $B(r)$=μ, where μ is the reduced mass. $R_{\rm out}$ is simply $e^2Z_dZ_\alpha/Q_\alpha$.

The decay constant is calculated using the theoretical or the experimental α decay half-life T_α by

$$\lambda=\frac{\ln 2}{T_\alpha}. \quad (12)$$

The preformation factor P_0 for the α cluster inside the mother nucleus is extracted by Eqs. (1), (2), (11), and (12).

3 Results and discussions

The α decay energy Q_α, the logarithmic half-life $\log_{10}(T_\alpha)$, the decay constant λ, the velocity ν, the assault frequency ν_0, the penetrability P, the preformation factor P_0 and the shell-pair correction energy E_{S+P} are given for the Po, Rn, Ra, Th, U isotopes and the N = 126, 128, 152, 162, 176, 184 isotones in Tables 1, 2, 3, 4, 5 and 6 respectively. The α decay energy Q_α and the logarithmic half-life $\log_{10}(T_\alpha)$ are experimental data. For some nuclei, when the experimental results do not exist, Q_α and E_{S+P} are adopted from the finite-range liquid drop model (FRDM) [35], and the half-life $\log_{10}(T_\alpha)$ was estimated by the following fomulas [36]:

$$\log_{10}[T_\alpha(s)]=-25.31-1.1629A^{1/6}\sqrt{Z}+\frac{1.5864Z}{\sqrt{Q_\alpha}}, \quad (13)$$

for even-even nuclei;

$$\log_{10}[T_\alpha(s)]=-26.65-1.0859A^{1/6}\sqrt{Z}+\frac{1.5848Z}{\sqrt{Q_\alpha}}, \quad (14)$$

for even-odd nuclei;

$$\log_{10}[T_\alpha(s)]=-25.68-1.1423A^{1/6}\sqrt{Z}+\frac{1.592Z}{\sqrt{Q_\alpha}}, \quad (15)$$

for odd-even nuclei; and

$$\log_{10}[T_\alpha(s)]=-29.48-1.113A^{1/6}\sqrt{Z}+\frac{1.6971Z}{\sqrt{Q_\alpha}}, \quad (16)$$

for odd-odd nuclei.

The decay constant may be deduced from the experimental α decay half-life T_α by $\lambda=\frac{\ln 2}{T_\alpha}$.

To study the correlation between the preformation factors and the structure properties, the preformation factors of N = 126 and 128 isotones are given as a function of the proton number Z in Fig. 1. For N = 126, as the proton number goes away from Z = 82, known as one of the proton magic numbers, to Z = 91, the preformation factor increases smoothly according to the rule of odd-even staggering, within the range of variation below 0.01 due to the spherical shell closure. Then the preformation factor rises abruptly until Z = 92, and after that its rate of increase speeds up, breaking the odd-even

Table 1. Characteristics of α formation and penetration for the N = 126 and N = 128 isotones. The first column indicates the proton number. The second and third columns correspond, respectively, to the neutron number and mass number. The fourth and the fifth columns correspond, respectively, to the experimental Q_α and $\log_{10}(T_\alpha)$. The sixth column is the decay constant λ. The seventh and eighth columns correspond, respectively, to the velocity and frequency of the α cluster inside the mother nucleus. The ninth column is the penetration probability and the last column gives the preformation factor extracted from Eq. (1) and the data of this table.

Z	N	A	Q_α/MeV	$\log_{10}(T_\alpha)$	$\lambda/{\rm s}^{-1}$	ν/(fm/s)	$\nu_0/{\rm s}^{-1}$	P	P_0
84	126	210	5.41	7.08	5.78×10^{-08}	1.58×10^{22}	1.14×10^{21}	7.87×10^{-27}	6.43×10^{-03}
85	126	211	5.98	4.79	1.12×10^{-05}	1.70×10^{22}	1.20×10^{21}	1.91×10^{-24}	4.87×10^{-03}
86	126	212	6.39	3.15	4.95×10^{-04}	1.80×10^{22}	1.24×10^{21}	4.14×10^{-23}	9.67×10^{-03}
87	126	213	6.91	1.54	1.99×10^{-02}	1.90×10^{22}	1.28×10^{21}	1.90×10^{-21}	8.18×10^{-03}
88	126	214	7.27	0.40	2.77×10^{-01}	2.00×10^{22}	1.32×10^{21}	1.70×10^{-20}	1.24×10^{-02}
89	126	215	7.74	-0.77	4.08×10^{00}	2.09×10^{22}	1.35×10^{21}	2.82×10^{-19}	1.07×10^{-02}
90	126	216	8.07	-1.57	2.57×10^{01}	2.15×10^{22}	1.38×10^{21}	1.32×10^{-18}	1.41×10^{-02}
91	126	217	8.49	-2.46	1.99×10^{02}	2.23×10^{22}	1.41×10^{21}	1.11×10^{-17}	1.27×10^{-02}
92	126	218	8.79	-3.29	1.35×10^{03}	2.27×10^{22}	1.44×10^{21}	3.45×10^{-17}	2.73×10^{-02}
93	126	219	9.18	-5.30	1.39×10^{05}	2.34×10^{22}	1.47×10^{21}	1.78×10^{-16}	5.31×10^{-01}
84	128	212	8.95	-6.52	2.31×10^{06}	2.31×10^{22}	1.46×10^{21}	4.91×10^{-14}	3.22×10^{-02}
85	128	213	9.25	-6.90	5.55×10^{06}	2.35×10^{22}	1.49×10^{21}	1.19×10^{-13}	3.13×10^{-02}
86	128	214	9.21	-6.57	2.57×10^{06}	2.34×10^{22}	1.48×10^{21}	4.51×10^{-14}	3.85×10^{-02}
87	128	215	9.54	-7.07	8.06×10^{06}	2.41×10^{22}	1.50×10^{21}	1.27×10^{-13}	4.21×10^{-02}
88	128	216	9.53	-6.74	3.85×10^{06}	2.40×10^{22}	1.50×10^{21}	5.72×10^{-14}	4.49×10^{-02}
89	128	217	9.83	-7.16	1.00×10^{07}	2.47×10^{22}	1.52×10^{21}	1.43×10^{-13}	4.62×10^{-02}
90	128	218	9.85	-6.96	6.30×10^{06}	2.46×10^{22}	1.52×10^{21}	7.60×10^{-14}	5.45×10^{-02}
91	128	219	10.08	-7.28	1.31×10^{07}	2.49×10^{22}	1.54×10^{21}	1.21×10^{-13}	7.03×10^{-02}
92	128	220	10.21	-7.22	1.16×10^{07}	2.50×10^{22}	1.54×10^{21}	1.13×10^{-13}	6.64×10^{-02}
93	128	221	10.36	-7.52	2.31×10^{07}	2.55×10^{22}	1.55×10^{21}	1.20×10^{-13}	1.24×10^{-01}

Table 2. Characteristics of α formation and penetration for the even-even Po, Rn, Ra and Th isotopes. The first column indicates the proton number. The second and third columns correspond, respectively, to the neutron number and mass number. The fourth and the fifth columns correspond, respectively, to the experimental Q_α and $\log_{10}(T_\alpha)$. The sixth column is the decay constant λ. The seventh and eighth columns correspond, respectively, to the velocity and frequency of the α cluster inside the mother nucleus. The ninth column is the penetration probability and the last column gives the preformation factor extracted from Eq. (1) and the data of this table.

Z	N	A	Q_α/MeV	$\log_{10}(T_\alpha)$	λ/s^{-1}	$\nu/(\mathrm{fm/s})$	ν_0/s^{-1}	P	P_0
84	106	190	7.69	-2.60	2.77×10^{02}	2.11×10^{22}	1.41×10^{21}	6.21×10^{-18}	3.17×10^{-02}
84	110	194	6.99	-0.41	1.78×10^{00}	1.97×10^{22}	1.33×10^{21}	3.29×10^{-20}	4.05×10^{-02}
84	112	196	6.66	0.77	1.17×10^{-01}	1.89×10^{22}	1.30×10^{21}	2.07×10^{-21}	4.37×10^{-02}
84	114	198	6.31	2.28	3.65×10^{-03}	1.81×10^{22}	1.26×10^{21}	8.51×10^{-23}	3.41×10^{-02}
84	116	200	5.98	3.79	1.12×10^{-04}	1.73×10^{22}	1.22×10^{21}	3.66×10^{-24}	2.50×10^{-02}
84	118	202	5.70	5.15	4.95×10^{-06}	1.69×10^{22}	1.19×10^{21}	1.81×10^{-25}	2.31×10^{-02}
84	120	204	5.49	6.28	3.65×10^{-07}	1.63×10^{22}	1.16×10^{21}	1.51×10^{-26}	2.08×10^{-02}
84	122	206	5.33	7.15	4.95×10^{-08}	1.57×10^{22}	1.14×10^{21}	2.24×10^{-27}	1.94×10^{-02}
84	124	208	5.22	7.96	7.62×10^{-09}	1.55×10^{22}	1.12×10^{21}	5.59×10^{-28}	1.21×10^{-02}
84	126	210	5.41	7.08	5.78×10^{-08}	1.58×10^{22}	1.14×10^{21}	7.87×10^{-27}	6.43×10^{-03}
84	128	212	8.95	-6.52	2.31×10^{06}	2.31×10^{22}	1.46×10^{21}	4.91×10^{-14}	3.22×10^{-02}
84	130	214	7.83	-3.80	4.33×10^{03}	2.07×10^{22}	1.36×10^{21}	4.63×10^{-17}	6.86×10^{-02}
84	132	216	6.91	-0.82	4.62×10^{00}	1.89×10^{22}	1.28×10^{21}	4.01×10^{-20}	9.02×10^{-02}
86	116	202	6.77	1.07	5.96×10^{-02}	1.92×10^{22}	1.29×10^{21}	1.05×10^{-21}	4.39×10^{-02}
86	118	204	6.55	2.04	6.30×10^{-03}	1.85×10^{22}	1.27×10^{21}	1.37×10^{-22}	3.62×10^{-02}
86	120	206	6.38	2.74	1.26×10^{-03}	1.82×10^{22}	1.25×10^{21}	3.05×10^{-23}	3.31×10^{-02}
86	122	208	6.26	3.38	2.89×10^{-04}	1.80×10^{22}	1.23×10^{21}	9.46×10^{-24}	2.48×10^{-02}
86	124	210	6.16	3.95	7.70×10^{-05}	1.75×10^{22}	1.22×10^{21}	4.05×10^{-24}	1.56×10^{-02}
86	126	212	6.39	3.15	4.95×10^{-04}	1.80×10^{22}	1.24×10^{21}	4.14×10^{-23}	9.67×10^{-03}
86	128	214	9.21	-6.57	2.57×10^{06}	2.34×10^{22}	1.48×10^{21}	4.51×10^{-14}	3.85×10^{-02}
86	130	216	8.20	-4.35	1.54×10^{04}	2.17×10^{22}	1.39×10^{21}	1.06×10^{-16}	1.05×10^{-01}
86	132	218	7.26	-1.46	1.98×10^{01}	1.96×10^{22}	1.31×10^{21}	1.30×10^{-19}	1.17×10^{-01}
86	134	220	6.41	1.75	1.24×10^{-02}	1.76×10^{22}	1.22×10^{21}	7.00×10^{-23}	1.45×10^{-01}
86	136	222	5.59	5.52	2.10×10^{-06}	1.59×10^{22}	1.14×10^{21}	1.09×10^{-26}	1.69×10^{-01}
88	116	204	7.64	-1.23	1.17×10^{01}	2.08×10^{22}	1.37×10^{21}	1.97×10^{-19}	4.35×10^{-02}
88	118	206	7.42	-0.62	2.89×10^{00}	2.05×10^{22}	1.35×10^{21}	3.74×10^{-20}	5.73×10^{-02}
88	120	208	7.27	0.14	5.07×10^{-01}	2.02×10^{22}	1.33×10^{21}	1.28×10^{-20}	2.97×10^{-02}
88	122	210	7.15	0.58	1.82×10^{-01}	1.97×10^{22}	1.31×10^{21}	5.51×10^{-21}	2.52×10^{-02}
88	124	212	7.03	1.16	4.80×10^{-02}	1.95×10^{22}	1.30×10^{21}	2.09×10^{-21}	1.77×10^{-02}
88	126	214	7.27	0.40	2.77×10^{-01}	2.00×10^{22}	1.32×10^{21}	1.70×10^{-20}	1.24×10^{-02}
88	128	216	9.53	-6.74	3.85×10^{06}	2.40×10^{22}	1.50×10^{21}	5.72×10^{-14}	4.49×10^{-02}
88	130	218	8.55	-4.59	2.67×10^{04}	2.24×10^{22}	1.42×10^{21}	2.08×10^{-16}	9.04×10^{-02}
88	132	220	7.59	-1.74	3.85×10^{01}	2.02×10^{22}	1.33×10^{21}	2.78×10^{-19}	1.04×10^{-01}
88	134	222	6.68	1.58	1.82×10^{-02}	1.84×10^{22}	1.24×10^{21}	1.31×10^{-22}	1.12×10^{-01}
88	136	224	5.79	5.52	2.10×10^{-06}	1.62×10^{22}	1.15×10^{21}	1.24×10^{-26}	1.46×10^{-01}
88	138	226	4.87	10.72	1.31×10^{-11}	1.44×10^{22}	1.06×10^{21}	7.31×10^{-32}	1.69×10^{-01}
90	120	210	8.05	-1.77	4.08×10^{01}	2.15×10^{22}	1.39×10^{21}	9.39×10^{-19}	3.12×10^{-02}
90	122	212	7.95	-1.44	1.93×10^{01}	2.12×10^{22}	1.38×10^{21}	4.80×10^{-19}	2.91×10^{-02}
90	124	214	7.83	-1.00	6.93×10^{00}	2.10×10^{22}	1.36×10^{21}	2.04×10^{-19}	2.50×10^{-02}
90	126	216	8.07	-1.57	2.57×10^{01}	2.15×10^{22}	1.38×10^{21}	1.32×10^{-18}	1.41×10^{-02}
90	128	218	9.85	-6.96	6.30×10^{06}	2.46×10^{22}	1.52×10^{21}	7.60×10^{-14}	5.45×10^{-02}
90	130	220	8.95	-5.01	7.15×10^{04}	2.28×10^{22}	1.45×10^{21}	5.46×10^{-16}	9.05×10^{-02}
90	132	222	8.13	-2.70	3.47×10^{02}	2.14×10^{22}	1.37×10^{21}	2.57×10^{-18}	9.82×10^{-02}
90	134	224	7.30	0.02	6.60×10^{-01}	1.97×10^{22}	1.30×10^{21}	4.60×10^{-21}	1.11×10^{-01}
90	136	226	6.45	3.26	3.85×10^{-04}	1.77×10^{22}	1.22×10^{21}	2.28×10^{-24}	1.39×10^{-01}
90	138	228	5.52	7.78	1.16×10^{-08}	1.57×10^{22}	1.12×10^{21}	5.87×10^{-29}	1.76×10^{-01}
90	140	230	4.77	12.38	2.89×10^{-13}	1.41×10^{22}	1.04×10^{21}	1.24×10^{-33}	2.24×10^{-01}

Table 3. Characteristics of α formation and penetration for the even-even U isotopes, extracted from both experimental efforts and theoretical models. The first column indicates the proton number. The second and third columns correspond, respectively, to the neutron number and mass number. The fourth and the fifth columns correspond, respectively, to the experimental Q_α and $\log_{10}(T_\alpha)$. The sixth column is the decay constant λ. The seventh and eighth columns correspond, respectively, to the velocity and frequency of the α cluster inside the mother nucleus. The ninth column is the penetration probability and the last column gives the preformation factor extracted from Eq. (1) and the data of this table.

Z	N	A	Q_α/MeV	$\log_{10}(T_\alpha)$	λ/s^{-1}	$\nu/(fm/s)$	ν_0/s^{-1}	P	P_0
92	124	216	8.53	-2.16	1.00×10^{02}	2.24×10^{22}	1.42×10^{21}	5.73×10^{-18}	1.23×10^{-02}
92	126	218	8.79	-3.26	1.26×10^{03}	2.27×10^{22}	1.44×10^{21}	3.45×10^{-17}	2.54×10^{-02}
92	128	220	10.21	-7.22	1.16×10^{07}	2.50×10^{22}	1.54×10^{21}	1.13×10^{-13}	6.64×10^{-02}
92	130	222	9.48	-5.33	1.47×10^{05}	2.40×10^{22}	1.48×10^{21}	2.68×10^{-15}	3.71×10^{-02}
92	132	224	8.62	-3.40	1.75×10^{03}	2.23×10^{22}	1.41×10^{21}	1.45×10^{-17}	8.55×10^{-02}
92	134	226	7.70	-0.57	2.58×10^{00}	2.07×10^{22}	1.33×10^{21}	2.17×10^{-20}	8.93×10^{-02}
92	136	228	6.80	2.74	1.27×10^{-03}	1.87×10^{22}	1.24×10^{21}	9.80×10^{-24}	1.04×10^{-01}
92	138	230	5.99	6.24	3.97×10^{-07}	1.65×10^{22}	1.16×10^{21}	2.05×10^{-27}	1.66×10^{-01}
92	140	232	5.41	9.34	3.19×10^{-10}	1.52×10^{22}	1.10×10^{21}	1.48×10^{-30}	1.95×10^{-01}
92	142	234	4.86	12.89	8.95×10^{-14}	1.44×10^{22}	1.04×10^{21}	4.15×10^{-34}	2.07×10^{-01}
92	144	236	4.57	14.87	9.37×10^{-16}	1.37×10^{22}	1.01×10^{21}	4.33×10^{-36}	2.15×10^{-01}
92	146	238	4.27	17.15	4.92×10^{-18}	1.32×10^{22}	9.71×10^{20}	1.62×10^{-38}	3.13×10^{-01}
92	114	206	9.26	-4.44	1.92×10^{04}	2.38×10^{22}	1.50×10^{21}	3.47×10^{-16}	3.68×10^{-02}
92	116	208	9.08	-4.01	7.14×10^{03}	2.34×10^{22}	1.48×10^{21}	1.33×10^{-16}	3.62×10^{-02}
92	118	210	8.62	-2.78	4.17×10^{02}	2.25×10^{22}	1.44×10^{21}	7.95×10^{-18}	3.64×10^{-02}
92	120	212	8.38	-2.11	9.03×10^{01}	2.21×10^{22}	1.42×10^{21}	1.67×10^{-18}	3.82×10^{-02}
92	122	214	8.46	-2.40	1.73×10^{02}	2.21×10^{22}	1.42×10^{21}	3.17×10^{-18}	3.85×10^{-02}
92	124	216	8.37	-2.17	1.02×10^{02}	2.19×10^{22}	1.41×10^{21}	1.84×10^{-18}	3.96×10^{-02}
92	126	218	8.52	-2.66	3.16×10^{02}	2.23×10^{22}	1.41×10^{21}	5.78×10^{-18}	3.86×10^{-02}
92	128	220	10.64	-7.96	6.35×10^{07}	2.58×10^{22}	1.58×10^{21}	8.33×10^{-13}	4.84×10^{-02}
92	130	222	9.15	-4.49	2.17×10^{04}	2.33×10^{22}	1.46×10^{21}	3.79×10^{-16}	3.93×10^{-02}
92	132	224	8.24	-1.94	6.03×10^{01}	2.18×10^{22}	1.38×10^{21}	1.03×10^{-18}	4.27×10^{-02}
92	134	226	7.62	0.05	6.18×10^{-01}	2.03×10^{22}	1.32×10^{21}	1.10×10^{-20}	4.25×10^{-02}
92	136	228	7.14	1.76	1.21×10^{-02}	1.94×10^{22}	1.27×10^{21}	2.07×10^{-22}	4.57×10^{-02}
92	138	230	6.18	5.81	1.07×10^{-06}	1.70×10^{22}	1.18×10^{21}	1.62×10^{-26}	5.57×10^{-02}
92	140	232	5.30	10.47	2.37×10^{-11}	1.51×10^{22}	1.09×10^{21}	2.86×10^{-31}	7.60×10^{-02}
92	142	234	4.68	14.50	2.18×10^{-15}	1.39×10^{22}	1.02×10^{21}	2.01×10^{-35}	1.06×10^{-01}
92	144	236	4.47	16.03	6.45×10^{-17}	1.35×10^{22}	9.96×10^{20}	6.24×10^{-37}	1.04×10^{-01}
92	146	238	4.10	19.05	6.25×10^{-20}	1.29×10^{22}	9.51×10^{20}	4.72×10^{-40}	1.39×10^{-01}
92	148	240	3.75	22.30	3.46×10^{-23}	1.23×10^{22}	9.07×10^{20}	1.95×10^{-43}	1.96×10^{-01}
92	150	242	3.52	24.69	1.41×10^{-25}	1.19×10^{22}	8.76×10^{20}	6.23×10^{-46}	2.59×10^{-01}
92	152	244	3.31	27.09	5.66×10^{-28}	1.15×10^{22}	8.47×10^{20}	2.42×10^{-48}	2.76×10^{-01}
92	154	246	3.49	24.95	7.79×10^{-26}	1.20×10^{22}	8.67×10^{20}	3.73×10^{-46}	2.41×10^{-01}
92	156	248	3.29	27.26	3.84×10^{-28}	1.16×10^{22}	8.40×10^{20}	1.44×10^{-48}	3.19×10^{-01}
92	158	250	2.62	36.95	7.84×10^{-38}	1.03×10^{22}	7.47×10^{20}	1.17×10^{-58}	8.95×10^{-01}

Table 4. The shell-pair effect correction factor $E(S+P)$ for the $N = 126$ and $N = 128$ isotones. The first column indicates the proton number. The second and third columns correspond, respectively, to the neutron number and mass number. The fourth column is the shell-pair effect correction factor.The last four columns are same as the first four columns.

Z	N	A	E_{S+P}	Z	N	A	E_{S+P}
80	126	206	-12.87	80	128	208	-10.8
81	126	207	-13.79	81	128	209	-11.71
82	126	208	-13.93	82	128	210	-11.85
83	126	209	-12.83	83	128	211	-10.82
84	126	210	-11.79	84	128	212	-9.74
85	126	211	-10.45	85	128	213	-8.44
86	126	212	-9.3	86	128	214	-7.29
87	126	213	-8.2	87	128	215	-6.21

Continued on next page

Table 4. – continued from previous page

Z	N	A	E_{S+P}	Z	N	A	E_{S+P}
88	126	214	-7.18	88	128	216	-5.2
89	126	215	-6.23	89	128	217	-4.27
90	126	216	-5.43	90	128	218	-3.47
91	126	217	-4.62	91	128	219	-3.85
92	126	218	-4.04	92	128	220	-3.63
93	126	219	-3.35	93	128	221	-3.24
94	126	220	-3	94	128	222	-2.87
95	126	221	-2.79	95	128	223	-2.47
96	126	222	-2.53	96	128	224	-2.24
97	126	223	-2.55	97	128	225	-2.08
98	126	224	-2.61	98	128	226	-1.99
99	126	225	-2.74	99	128	227	-2.75
100	126	226	-2.96	100	128	228	-2.69

Table 5. Characteristics of α formation and penetration for the $N = 152$ and 162 isotones. The first column indicates the proton number. The second and third columns correspond, respectively, to the neutron number and mass number. The fourth and the fifth columns correspond, respectively, to the experimental Q_α and $\log_{10}(T_\alpha)$. The sixth column is the decay constant λ. The seventh and eighth columns correspond, respectively, to the velocity and frequency of the α cluster inside the mother nucleus. The ninth column is the penetration probability and the tenth column gives the preformation factor extracted from Eq. (1) and the data of this table. The last column is the shell-pair effect correction factor E_{S+P}.

Z	N	A	Q_α/MeV	$\log_{10}(T_\alpha)$	λ/s^{-1}	$\nu/(\mathrm{fm/s})$	ν_0/s^{-1}	P	P_0	E_{S+P}
96	152	248	5.35	11.98	7.18×10^{-13}	1.50×10^{22}	1.07×10^{21}	9.49×10^{-33}	7.06×10^{-02}	-5.24
97	152	249	5.73	10.62	1.65×10^{-11}	1.55×10^{22}	1.11×10^{21}	5.70×10^{-31}	2.61×10^{-02}	-5.81
98	152	250	6.26	7.94	7.91×10^{-09}	1.64×10^{22}	1.16×10^{21}	1.35×10^{-28}	5.07×10^{-02}	-5.93
99	152	251	6.77	6.36	3.05×10^{-07}	1.78×10^{22}	1.20×10^{21}	1.32×10^{-26}	1.93×10^{-02}	-6.42
100	152	252	7.25	4.39	2.83×10^{-05}	1.91×10^{22}	1.24×10^{21}	5.82×10^{-25}	3.92×10^{-02}	-6.45
101	152	253	7.90	2.66	1.51×10^{-03}	2.07×10^{22}	1.29×10^{21}	8.52×10^{-23}	1.37×10^{-02}	-6.74
102	152	254	8.47	0.74	1.26×10^{-01}	2.17×10^{22}	1.34×10^{21}	3.32×10^{-21}	2.84×10^{-02}	-6.55
103	152	255	8.81	0.38	2.91×10^{-01}	2.23×10^{22}	1.36×10^{21}	1.78×10^{-20}	1.20×10^{-02}	-6.92
104	152	256	9.27	-1.00	6.92×10^{00}	2.32×10^{22}	1.39×10^{21}	2.04×10^{-19}	2.43×10^{-02}	-6.36
105	152	257	9.56	-1.13	9.25×10^{00}	2.38×10^{22}	1.41×10^{21}	6.50×10^{-19}	1.01×10^{-02}	-6.82
106	152	258	9.87	-1.99	6.74×10^{01}	2.44×10^{22}	1.44×10^{21}	2.24×10^{-18}	2.09×10^{-02}	-6.61
107	152	259	10.30	-2.43	1.87×10^{02}	2.49×10^{22}	1.46×10^{21}	1.48×10^{-17}	8.59×10^{-03}	-7.02
108	152	260	10.95	-4.06	7.98×10^{03}	2.59×10^{22}	1.51×10^{21}	2.66×10^{-16}	1.99×10^{-02}	-6.28
109	152	261	11.58	-4.83	4.69×10^{04}	2.69×10^{22}	1.55×10^{21}	3.16×10^{-15}	9.58×10^{-03}	-6.22
110	152	262	12.17	-6.14	9.49×10^{05}	2.79×10^{22}	1.59×10^{21}	2.82×10^{-14}	2.12×10^{-02}	-5.53
111	152	263	12.87	-6.88	5.27×10^{06}	2.87×10^{22}	1.63×10^{21}	2.91×10^{-13}	1.11×10^{-02}	-5.16
112	152	264	13.28	-7.72	3.65×10^{07}	2.94×10^{22}	1.65×10^{21}	8.41×10^{-13}	2.62×10^{-02}	-4.22
100	162	262	5.61	12.26	3.79×10^{-13}	1.51×10^{22}	1.08×10^{21}	6.32×10^{-33}	5.57×10^{-02}	-5.06
101	162	263	5.97	11.08	5.76×10^{-12}	1.57×10^{22}	1.11×10^{21}	2.59×10^{-31}	2.01×10^{-02}	-5.67
102	162	264	6.46	8.62	1.67×10^{-09}	1.64×10^{22}	1.15×10^{21}	3.52×10^{-29}	4.13×10^{-02}	-6.15
103	162	265	6.77	7.97	7.45×10^{-09}	1.70×10^{22}	1.18×10^{21}	4.06×10^{-28}	1.56×10^{-02}	-6.81
104	162	266	7.20	6.11	5.38×10^{-07}	1.82×10^{22}	1.21×10^{21}	1.33×10^{-26}	3.34×10^{-02}	-7.39
105	162	267	7.58	5.34	3.17×10^{-06}	1.96×10^{22}	1.24×10^{21}	2.00×10^{-25}	1.27×10^{-02}	-8.08
106	162	268	8.05	3.56	1.89×10^{-04}	2.07×10^{22}	1.28×10^{21}	5.35×10^{-24}	2.76×10^{-02}	-8.18
107	162	269	8.54	2.60	1.76×10^{-03}	2.18×10^{22}	1.32×10^{21}	1.26×10^{-22}	1.06×10^{-02}	-8.74
108	162	270	9.09	0.80	1.10×10^{-01}	2.28×10^{22}	1.36×10^{21}	3.55×10^{-21}	2.29×10^{-02}	-9.07
109	162	271	9.69	-0.27	1.28×10^{00}	2.38×10^{22}	1.40×10^{21}	1.05×10^{-19}	8.73×10^{-03}	-9.42
110	162	272	10.36	-2.13	9.46×10^{01}	2.48×10^{22}	1.44×10^{21}	3.85×10^{-18}	1.70×10^{-02}	-9.07
111	162	273	11.14	-3.38	1.68×10^{03}	2.63×10^{22}	1.50×10^{21}	1.59×10^{-16}	7.07×10^{-03}	-8.89
112	162	274	11.72	-4.77	4.09×10^{04}	2.70×10^{22}	1.53×10^{21}	1.56×10^{-15}	1.71×10^{-02}	-8.75
113	162	275	12.25	-5.24	1.21×10^{05}	2.78×10^{22}	1.56×10^{21}	9.80×10^{-15}	7.90×10^{-03}	-8.1
114	162	276	12.73	-6.30	1.38×10^{06}	2.87×10^{22}	1.59×10^{21}	4.32×10^{-14}	2.01×10^{-02}	-7.39
115	162	277	13.05	-6.27	1.30×10^{06}	2.90×10^{22}	1.61×10^{21}	8.82×10^{-14}	9.13×10^{-03}	-7.25
116	162	278	13.04	-6.34	1.53×10^{06}	2.89×10^{22}	1.61×10^{21}	4.66×10^{-14}	2.04×10^{-02}	-5.21

Table 6. Characteristics of α formation and penetration for the $N = 176$ and 184 isotones. The first column indicates the proton number. The second and third columns correspond, respectively, to the neutron number and mass number. The fourth and the fifth columns correspond, respectively, to the experimental Q_α and $\log_{10}(T_\alpha)$. The sixth column is the decay constant λ. The seventh and eighth columns correspond, respectively, to the velocity and frequency of the α cluster inside the mother nucleus. The ninth column is the penetration probability and the tenth column gives the preformation factor extracted from Eq. (1) and the data of this table. The last column is the shell-pair effect correction factor E_{S+P}.

Z	N	A	Q_α/MeV	$\log_{10}(T_\alpha)$	λ/s^{-1}	$\nu/(fm/s)$	ν_0/s^{-1}	P	P_0	E_{S+P}
104	176	280	5.60	14.09	5.66×10^{-15}	1.51×10^{22}	1.05×10^{21}	8.37×10^{-35}	6.44×10^{-02}	-4.37
105	176	281	5.96	12.85	9.89×10^{-14}	1.56×10^{22}	1.08×10^{21}	4.30×10^{-33}	2.13×10^{-02}	-4.89
106	176	282	6.52	9.90	8.81×10^{-11}	1.63×10^{22}	1.13×10^{21}	2.08×10^{-30}	3.74×10^{-02}	-5.19
107	176	283	6.84	9.19	4.52×10^{-10}	1.69×10^{22}	1.16×10^{21}	2.94×10^{-29}	1.33×10^{-02}	-5.84
108	176	284	7.26	7.30	3.46×10^{-08}	1.74×10^{22}	1.19×10^{21}	9.66×10^{-28}	3.01×10^{-02}	-6.28
109	176	285	7.72	6.19	4.50×10^{-07}	1.79×10^{22}	1.23×10^{21}	3.42×10^{-26}	1.07×10^{-02}	-6.85
110	176	286	8.05	4.90	8.82×10^{-06}	2.03×10^{22}	1.25×10^{21}	2.82×10^{-25}	2.50×10^{-02}	-7.34
111	176	287	8.45	4.21	4.29×10^{-05}	2.12×10^{22}	1.28×10^{21}	3.74×10^{-24}	8.95×10^{-03}	-7.66
112	176	288	8.89	2.66	1.51×10^{-03}	2.23×10^{22}	1.31×10^{21}	5.64×10^{-23}	2.05×10^{-02}	-7.75
113	176	289	9.11	2.71	1.36×10^{-03}	2.28×10^{22}	1.33×10^{21}	1.36×10^{-22}	7.57×10^{-03}	-8.39
114	176	290	9.14	2.57	1.86×10^{-03}	2.28×10^{22}	1.33×10^{21}	7.65×10^{-23}	1.83×10^{-02}	-8.95
115	176	291	10.04	0.57	1.86×10^{-01}	2.44×10^{22}	1.39×10^{21}	2.15×10^{-20}	6.24×10^{-03}	-9.14
116	176	292	11.12	-2.38	1.67×10^{02}	2.60×10^{22}	1.46×10^{21}	8.16×10^{-18}	1.40×10^{-02}	-8.77
117	176	293	11.70	-3.06	8.03×10^{02}	2.69×10^{22}	1.50×10^{21}	1.04×10^{-16}	5.17×10^{-03}	-8.84
118	176	294	12.67	-5.29	1.35×10^{05}	2.83×10^{22}	1.55×10^{21}	5.67×10^{-15}	1.53×10^{-02}	-8.6
119	176	295	13.24	-5.76	4.01×10^{05}	2.92×10^{22}	1.59×10^{21}	3.76×10^{-14}	6.72×10^{-03}	-8.96
120	176	296	13.89	-7.11	9.01×10^{06}	2.99×10^{22}	1.62×10^{21}	2.84×10^{-13}	1.96×10^{-02}	-8.24
121	176	297	14.77	-8.01	7.09×10^{07}	3.11×10^{22}	1.67×10^{21}	3.92×10^{-12}	1.08×10^{-02}	-7.78
122	176	298	15.46	-9.28	1.32×10^{09}	3.21×10^{22}	1.71×10^{21}	2.21×10^{-11}	3.49×10^{-02}	-6.8
123	176	299	15.29	-8.36	1.59×10^{08}	3.19×10^{22}	1.70×10^{21}	7.64×10^{-12}	1.22×10^{-02}	-5.82
124	176	300	15.29	-8.50	2.21×10^{08}	3.19×10^{22}	1.70×10^{21}	4.55×10^{-12}	2.87×10^{-02}	-5.82
106	184	290	5.39	16.33	3.24×10^{-17}	1.49×10^{22}	1.02×10^{21}	4.47×10^{-37}	7.11×10^{-02}	-3.58
107	184	291	5.68	15.39	2.83×10^{-16}	1.52×10^{22}	1.04×10^{21}	1.19×10^{-35}	2.28×10^{-02}	-4.06
108	184	292	6.18	12.49	2.23×10^{-13}	1.59×10^{22}	1.09×10^{21}	4.15×10^{-33}	4.94×10^{-02}	-4.64
109	184	293	6.52	11.55	1.94×10^{-12}	1.65×10^{22}	1.12×10^{21}	1.27×10^{-31}	1.37×10^{-02}	-5.28
110	184	294	6.94	9.49	2.25×10^{-10}	1.70×10^{22}	1.15×10^{21}	6.17×10^{-30}	3.17×10^{-02}	-5.94
111	184	295	7.31	8.64	1.60×10^{-09}	1.74×10^{22}	1.18×10^{21}	1.26×10^{-28}	1.07×10^{-02}	-6.7
112	184	296	7.73	6.83	1.02×10^{-07}	1.79×10^{22}	1.21×10^{21}	3.36×10^{-27}	2.50×10^{-02}	-7.45
113	184	297	8.32	5.33	3.24×10^{-06}	2.08×10^{22}	1.25×10^{21}	3.06×10^{-25}	8.43×10^{-03}	-8.11
114	184	298	8.96	3.02	6.55×10^{-04}	2.24×10^{22}	1.30×10^{21}	2.59×10^{-23}	1.94×10^{-02}	-8.69
115	184	299	9.99	0.57	1.85×10^{-01}	2.41×10^{22}	1.37×10^{21}	2.05×10^{-20}	6.61×10^{-03}	-8.79
116	184	300	11.56	-3.59	2.68×10^{03}	2.65×10^{22}	1.47×10^{21}	1.24×10^{-16}	1.47×10^{-02}	-8.24
117	184	301	12.24	-4.42	1.83×10^{04}	2.76×10^{22}	1.51×10^{21}	1.86×10^{-15}	6.50×10^{-03}	-8.1
118	184	302	12.92	-5.95	6.14×10^{05}	2.86×10^{22}	1.55×10^{21}	2.13×10^{-14}	1.86×10^{-02}	-7.29
119	184	303	13.41	-6.24	1.20×10^{06}	2.94×10^{22}	1.58×10^{21}	1.05×10^{-13}	7.21×10^{-03}	-7.08
120	184	304	13.85	-7.19	1.06×10^{07}	2.99×10^{22}	1.61×10^{21}	3.56×10^{-13}	1.86×10^{-02}	-6.28
121	184	305	14.41	-7.53	2.36×10^{07}	3.08×10^{22}	1.64×10^{21}	1.60×10^{-12}	9.02×10^{-03}	-5.94
122	184	306	14.92	-8.54	2.43×10^{08}	3.13×10^{22}	1.66×10^{21}	5.53×10^{-12}	2.64×10^{-02}	-5.04
123	184	307	15.48	-8.81	4.50×10^{08}	3.21×10^{22}	1.69×10^{21}	2.02×10^{-11}	1.31×10^{-02}	-4.54
124	184	308	16.02	-9.81	4.49×10^{09}	3.27×10^{22}	1.72×10^{21}	6.38×10^{-11}	4.10×10^{-02}	-3.52
125	184	309	16.65	-10.11	9.03×10^{09}	3.36×10^{22}	1.75×10^{21}	2.37×10^{-10}	2.18×10^{-02}	-2.78
126	184	310	11.28	0.25	3.89×10^{-01}	2.62×10^{22}	1.44×10^{21}	3.36×10^{-20}	8.02×10^{-03}	-5.31
127	184	311	11.73	-0.15	9.77×10^{-01}	2.70×10^{22}	1.47×10^{21}	2.35×10^{-19}	2.84×10^{-03}	-5.62

staggering. The preformation factor for $N = 128$ isotones, whose variation resembles $N = 126$ isotones, increases slightly before $Z = 91$, but decreases a little bit and increases drastically when Z goes from 92 to 93. This casts doubt on the statement that the $N = 126$ shell closure effect influences the α particle preformation when $Z = 92$.

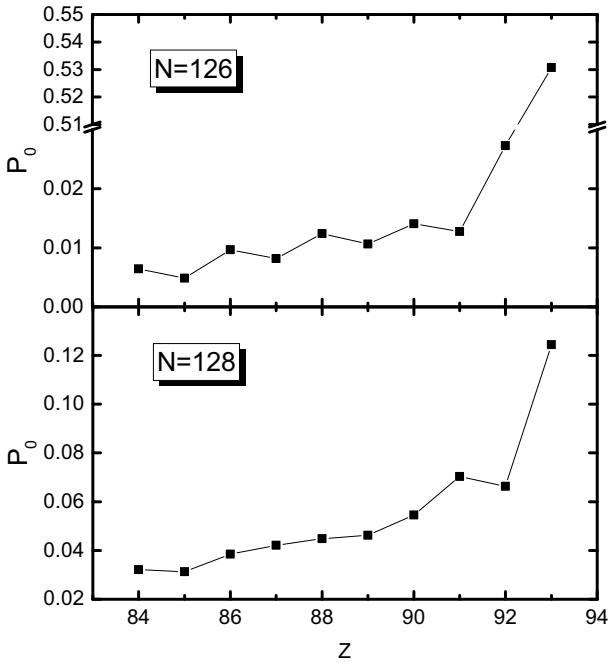

Fig. 1. Extracted preformation factors for the isotones of $N = 126$ and $N = 128$.

The changes of the preformation factors of even-even nuclei for Po, Rn, Ra, Th and U isotopes with increasing neutron number N are presented in Fig. 2. For the calculations above, we use the formulas given by fitting the preformation factors, which are extracted based on the differences between experimental and theoretical T_α[31]. Except for the U isotopes, they show a uniform downward trend until the spherical shell closure at $N = 126$, where the minimum of P_0 occurs, and then they increase sharply. It can be observed that the value is always at a minimum for the Po, Rn, Ra, and Th isotopes when $N = 126$, indicating that $N = 126$ is a magic number for such nuclei. However, for the U isotopes, where the preformation factors extracted from experimental data and calculated within theoretical models are shown, the trend changes. The minimum of neither line is at $N = 126$, in contrast to those of the Po, Rn, Ra and Th isotopes, which further confirms the weakness of $N = 126$ subshell closure when $Z = 92$. One can also find that the N=126 shell closure is evidently weakened, which is consistent with the recent experimental results [37, 38]. It is also worth noting that, except for the numerical difference of experimental and theoretical preformation factors of U isotopes in Fig. 2, the variation trends are almost the same. Therefore, the magic numbers predicted by the theoretically calculated P_0 in the region of superheavy nuclei are accurate to a certain extent.

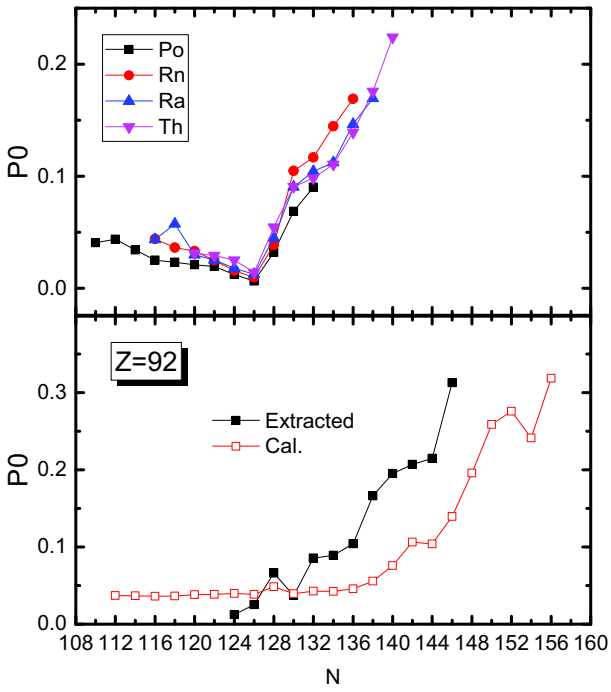

Fig. 2. (color online) Extracted preformation factors for the even-even isotopes of Po, Rn, Ra, and Th, and both extracted and calculated preformation factors for the even-even isotopes of U.

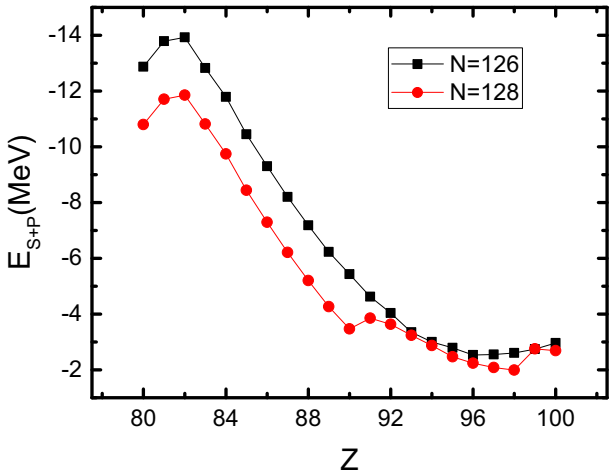

Fig. 3. (color online) Extracted shell-pair effect correction factors E_{S+P} for the isotones of $N = 126$ and $N = 128$.

The values of the shell effect correction factors E_{S+P} for the $N = 126$ and $N = 128$ isotones are plotted in Fig. 3. They rise to -14 MeV and -12 MeV respectively at $Z = 82$ at the beginning, and then both drop

and reach a minimum around $Z = 98$, after which they rise back. As E_{S+P} always increases when the proton and neutron numbers get close to the magic numbers, the second rise of E_{S+P} around $Z = 98$ clearly manifests that other proton magic numbers may exist after that.

To explore the proton magic numbers of superheavy nuclei, the values of the preformation factors for the N = 152, 162, 176, 184 isotones calculated by the theoretical Q_α and $\log_{10}(T_\alpha)$, and the shell effect correction factors E_{S+P} extracted from the liquid-drop model [36], are plotted respectively as a function of the proton number Z in Fig. 4. On the whole, the preformation factors of the four isotones above are all distributed between 0.001 and 0.07. The very low values show the possible presence of subshell closure when N = 152, 162, 176, 184. The preformation factors of the N = 152 and 162 isotones both decrease smoothly in the beginning and reach a minimum in the vicinity of Z = 108, but rise back afterwards, indicating that magic numbers may occur around $Z = 108$ for these two isotones. Similarly, the preformation factors of the $N = 176$ and 184 isotones decrease until Z = 116, increase from Z = 116 to 122 and Z = 116 to 124 respectively, then finally both fall again, which indicates that more than one magic number may exist for the $N = 176$ and 184 isotones. One is near Z = 116, and the other may occur after $Z = 124$. The changing trend of the shell effect correction factors strongly resembles that of the preformation factors. The minima of these two parameters occur at almost the same proton number. Thus, the theoretical calculations are reliable.

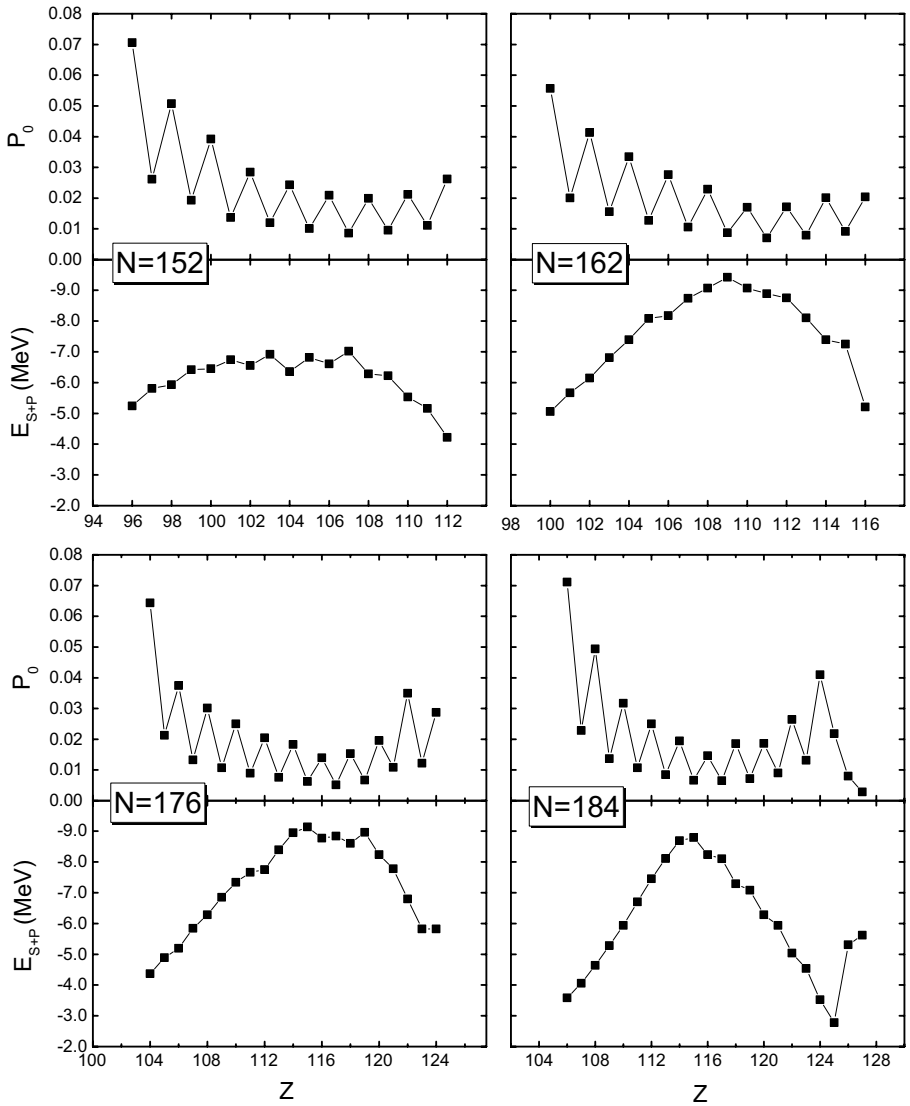

Fig. 4. Calculated preformation factors and extracted shell-pair effect correction factors E_{S+P} for the isotones of N = 152, N = 162, N = 176 and N = 184.

4 Summary

A study of the α preformation and shell effect of various nuclei has been presented. The decay constants are calculated from the decay half-lives. The penetration probabilities are calculated within the WKB approximation and the penetration barriers are built with the GLDM. Using a classical method to calculate the assault frequencies, the preformation factors can be extracted systematically. Clearly the shell closure effect plays a key role in the preformation mechanism. The closer the proton and nucleon numbers are to the magic numbers, the more difficult the preformation of α cluster inside the mother nucleus is. $N = 126$ is a magic number for the even-even nuclei when $Z = 84 - 90$, but for U isotopes, the $N = 126$ shell closure effect is reduced too much. We extend the study to the superheavy nuclei. As the shell closure effect is also an important feature of the superheavy nuclei, the magic numbers can be predicted by preformation factors and inspected by the shell effect correction factors. Subshell closure probably exists near $Z = 108$ when $N = 152$, 162 and $Z = 116$ when $N = 176$, 184. Meanwhile, other magic numbers may occur after $Z = 124$ in superheavy nuclei. It is interesting and necessary to study the preformation factors microscopically and systematically. There is a strong desire to further study the odd-odd and odd A nuclei and extract analytical formulas of preformation factors, which should be related to the α decay energy and the nucleon numbers. Further research on superheavy nuclei by studying α particle preformation is proposed, which could be very helpful to relevant experiments.

References

1 Z. Ren and G. Xu, Phys. Rev. C, **36**: 456 (1987)
2 R. G. Lovas, R. J. Liotta, A. Insolia, K. Varga, and D. S.Delion, Phys. Rep., **294**: 265 (1998)
3 F. Garcia, O. Rodriguez, M. Gonalves, S. B. Duarte, O. A. P. Tavares, and F. Guzman, J. Phys. G, **26**: 755 (2000)
4 G. Audi, O. Bersillon, J. Blachot, and A. H. Wapstra, Nucl. Phys. A, **729**: 3 (2003)
5 T. N. Ginter et al, Phys. Rev. C, **67**: 064609 (2003)
6 P. E. Hodgson and E. Betak, Phys. Rep., **374**: 1 (2003)
7 Z. G. Gan, J. S. Guo, X. L. Wu, Z. Qin, H. M. Fan, X. G. Lei, H. Y. Liu, B. Guo, H. G. Xu, R. F. Chen, C. F. Dong, F. M. Zhang, H. L. Wang, C. Y. Xie, Z. Q. Feng, Y. Zhen, L. T. Song, P. Luo, H. S. Xu, X. H. Zhou, G. M. Jin, and Z. Ren, Eur. Phys. J. A, **20**: 385 (2004)
8 D. Seweryniak et al, Phys. Rev. C, **73**: 061301(R) (2006)
9 A. P. Lepp ¨ anen et al, Phys. Rev. C, **75**: 054307 (2007)
10 Yu. Ts. Oganessian et al, Phys. Rev. C, **72**: 034611 (2005); **74**: 044602 (2006)
11 P. Schuck, Y. Funaki, H. Horiuchi, G. Rpke, A. Tohsaki, and T. Yamada, Nuclear Physics A, **738**(Supplement C): 245 94-100 (2004)
12 K. Morita et al, J. Phys. Soc. Jpn., **76**: 045001 (2007)
13 Yu. Ts. Oganessian et al, Phys. Rev. C, **76**: 011601(R) (2007)
14 G. Gamow, Z. Phys., **51**: 204 (1928)
15 E. U. Condon and R. W. Gurney, Nature (London), **122**: 439 (1928)
16 B. Buck, A. C. Merchant, and S. M. Perez, At. Data Nucl. Data Tables, **54**: 53 (1993)
17 P. Mohr, Phys. Rev. C, **73**: 031301(R) (2006)
18 D. N. Poenaru and M. Ivascu, Rev. Roum. Phys., **28**: 309 (1983)
19 K. Varga, R. G. Lovas, and R. J. Liotta, Phys. Rev. Lett., **69**: 37 (1992)
20 G. Royer and B. Remaud, Nucl. Phys. A, **444**: 447 (1985)
21 S. B. Duarte et al, At. Data Nucl. Data Tables, **80**: 235 (2002)
22 D. N. Basu, Phys. Lett. B, **566**: 90 (2003); P. Roy Chowdhury, D. N. Basu, and C. Samanta, Phys. Rev. C, **75**: 047306 (2007)
23 B. A. Brown, Phys. Rev. C, **46**: 811 (1992)
24 G. Royer, J. Phys. G, **26**: 1149 (2000); G. Royer and R. Moustabchir, Nucl. Phys. A, **683**: 182 (2001)
25 R. K. Gupta, M. Balasubramaniam, C. Mazzocchi, M. LaCommara, W. Scheid, Phys. Rev. C, **65**: 024201 (2002)
26 D. N. Poenaru, I. H. Plonski, and W. Greiner, Phys. Rev. C, **74**: 014312 (2006)
27 H. F. Zhang, W. Zuo, J. Q. Li, and G. Royer, Phys. Rev. C, **74**: 017304 (2006)
28 H. F. Zhang and G. Royer, Phys. Rev. C, **76**: 047304 (2007)
29 C. Xu and Z. Z. Ren, Phys. Rev. C, **74**: 014304 (2006); Nucl. Phys. A, **760**: 303 (2005)
30 J. C. Pei, F. R. Xu, Z. J. Lin, and E. G. Zhao, Phys. Rev. C, **76**: 044326 (2007)
31 H. F. Zhang and G. Royer, Phys. Rev. C, **77**: 054318 (2008)
32 L. Ma, Z. Y. Zhang, Z. G. Gan, H. B. Yang, L. Yu, J. Jiang, J. G. Wang, Y. L. Tian, Y. S. Wang, and S. Guo, Phys. Rev. C, **91**: (2015)
33 M. Sun, Z. Liu, T. H. Huang et al, Physics Letters B, **771**: 303 (2017)
34 G. Royer, J. Phys. G: Nucl. Part. Phys., **26** (2000)
35 P. Moller, A. J. Sierk, T. Ichikawa, and H. Sagawa, Atomic Data and Nuclear Data Tables, **109**: 110 (2016)
36 G. Royer, Journal of Physics G Nuclear Particle Physics, **26**: 1149 (2000)
37 J. Khuyagbaatar, A. Yakushev, Ch. E. Düllmann et al, Physical Review Letters, **115**: 242502 (2015)
38 R. Ferrer, A. Barzakh, B. Bastin et al, Nature Communications, **8**: 14520 (2017)